than the π interaction; i.e., reduction of repulsion is more important than attractive bond formation.

There is a clear distinction between the 1-fold adsorption on the one hand and 2- and 3-fold adsorption on the other. All interactions seem to be much weaker for the 1-fold adsorption. Due to the bend in the connection Ir–C–O for the 2- and 3-fold adsorption, there is a very favorable overlap between the $2\pi^*$ orbitals of CO and metal d orbitals. This gives rise to relatively strong bonds as can be seen in Figures 4 and 5. For the 1-fold adsorption this overlap is small and hardly any bond is formed. The preference for 2- and 3-fold adsorption is probably cluster size dependent. The strong repulsion for the 2- and 3-fold adsorption causes the 4σ level to participate. Two molecular orbitals are formed with about equal amounts of 4σ and 5σ character and little metal character. The participation of the 4σ orbital can clearly be seen in UPS spectra, e.g., compare the spectra of $Ir_4(CO)_{12}$ and CO–Ir(100).

The Mg^{2+} ion has two opposing effects on the CO adsorption. It polarizes the metal cluster pulling electrons away from the side where CO is to adsorb. This reduces the repulsion with the 5σ orbital but also makes the π back-donation more difficult. The net effect is that there is no change in the adsorption energy. The π back-donation is hampered most for the 1-fold adsorption where the electrons have to move farthest away from the cation. The change is most clearly shown by the occupation of the $2\pi^*$ orbitals. The occupation of the 5σ orbital changes little. The reduced overlap results in a slightly higher 5σ orbital occupation. The decrease of the occupation of the $2\pi^*$ orbitals will make it harder for CO to dissociate.

The Mg^{2+} ion does cause some changes in the structure and the vibrational properties. The distance between the CO molecule and the metal is increased. As the adsorption energy does not change, the potential minimum becomes flatter. This is reflected by a decrease of the Ir–C stretch frequencies. The C–O stretch frequencies increase due to the depopulation of the $2\pi^*$ orbitals.

There is an important difference between the geometries we have studied and geometries in which the cation sits next to CO on a metal surface. Electrostatic considerations show that in the latter case the CO orbitals are stabilized with respect to the metal orbitals. Via this mechanism the $2\pi^*$ orbitals can become more populated and dissociation possible. The reverse happens in our case. We note that, although the electrostatic effect of the cation is most important, there is some covalent interaction as well. The position of the cation may be inferred from vibrational spectra as cations close to CO decrease the C–O stretch frequency, whereas when the metal cluster is between the cation and CO the frequency is increased. The position of the cation, as determined by the zeolite structure and the cation size, may explain the catalytic properties of metal clusters in zeolites X, Y, and L as a function of the cation type.

Effect of the Electrical Double Layer on Voltammetry at Microelectrodes

John D. Norton, Henry S. White,*

Department of Chemical Engineering and Materials Science, University of Minnesota, Minneapolis, Minnesota 55455

and Stephen W. Feldberg

Brookhaven National Laboratory, Upton, New York 11973 *(Received: October 2, 1989; In Final Form: April 2, 1990)*

An analysis of transport of charged and uncharged species associated with a steady-state faradaic process at a spherical microelectrode is reported. We examine systems comprising various relative concentrations of a redox species and, if charged, its counterion and an inert electrolyte. Of particular interest is the behavior of these systems when the thickness of the diffuse double layer (characterized by the Debye length, κ^{-1}) and the radius of the electrode (r_0) are comparable. Transport of each species is assumed to be governed by the Nernst–Planck equation. A generalized solution obtained by using finite-difference simulations demonstrates that significant enhancement or inhibition of the steady-state flux can occur and will depend upon the dimensionless parameter $r_0\kappa$, upon the relative values of the applied potential (E_{app}), the formal redox potential ($E^{\circ\prime}$), and the potential of zero charge (E_{pzc}), upon the charges and relative concentrations of the species in solution, and upon the distance of closest approach of the reactant to the electrode surface. Analytic solutions for several limiting cases are discussed and serve as simple expositions of the phenomena as well as a verification of the simulations. In infinitely dilute ionic solutions, i.e., $r_0\kappa \rightarrow 0$, the limiting flux of ionic species may be computed directly from the Smoluchowski–Debye theory for ionic bimolecular reaction rates. Computation of theoretical voltammograms in the limit of infinite dilution (i.e., $r_0\kappa \rightarrow 0$) reveals the surprising result that under certain conditions the steady-state current–voltage curve will be peaked rather than sigmoidal, giving the appearance that electrochemical activity occurs only within a small (several hundred millivolt) potential window. The effect is easily explained when the electric field and the charge of the reacting species are considered.

Introduction

Development of electrochemical applications of microelectrodes has flourished during the last decade, expanding considerably beyond early applications as biological simulators and sensors.[1,2] It is now possible to produce a microelectrode or microelectrode array whose critical dimension, r_0 (e.g., the half-width of a band electrode or the radius of its hemicylindrical approximation; the radius of a disk electrode or its hemispherical approximation), is of the order of several nanometers.[3,4] Since the size of an electrode dictates the spatial (as well as the time) domain that is probed, the measurement of faradaic currents at an electrode with nanometer dimensions may reveal fundamental information about the solvent structure and potential distribution within a few

(1) Adams, R. N. *Anal. Chem.* **1976**, *48*, 1128A.
(2) Wightman, R. M. *Anal. Chem.* **1981**, *53*, 1125A.
(3) Morris, R. B.; Franta, D. J.; White, H. S. *J. Phys. Chem.* **1987**, *91*, 3559.
(4) Seibold, J. D.; Scott, E. R.; White, H. S. *J. Electroanal. Chem.* **1989**, *264*, 281.

0022-3654/90/2094-6772$02.50/0

tenths of a nanometer of the electrode surface.

When a faradaic reaction, e.g., $A^+ + e^- \rightarrow A$, occurs at an electrode a thin depletion layer is established in the solution adjacent to the electrode as a consequence of the finite rate at which the reactant can be transported from the bulk to the surface.[5] For a microelectrode having an $r_0 \leq 10^{-5}$ cm, the thickness of the depletion layer, δ, may be comparable to the thickness of the electrical double layer that is established in response to electrical charging of the electrode. It is thus meaningful (and necessary) to ask how the electric fields at the electrode surface will affect the fluxes and spatial distributions of various solution ions during an electrochemical measurement using a microelectrode.

The thicknesses of the electrical double layer and depletion layer have different dependencies on the electrode radius, r_0, and the chemical composition of the electrolyte. At equilibrium (i.e., when no net current is passing across the electrode/solution interface), the Debye length, κ^{-1}, is frequently used to characterize the thickness of the electrical double layer. In a solution containing an electrolyte, κ^{-1} is proportional to the inverse square root of the ionic concentration, $C^{-1/2}$, and independent of the electrode radius, r_0, or geometry.[5] Conversely, when a net current flows across the interface, a depletion layer develops which has a thickness, δ, that is defined as the distance away from the electrode surface at which the reactant (or product) is present at an arbitrarily chosen concentration that closely approximates its bulk value far from the electrode surface.[5] The precise value of δ is a complex function of mechanism of transport (migration, diffusion, and/or convection) and electrode geometry and may also be a function of time for certain electrode geometries where a steady-state response does not exist (e.g., planar electrode).[5] Thus, unlike the use of κ^{-1} for characterizing the electrical double layer thickness at equilibrium, there is no single parameter that is generally useful for characterizing δ for all electrode systems. Therefore, we limit our discussion in this report to spherical microelectrodes for which a true steady-state current response is predicted. In addition, in the absence of convective flow, transport of electroactive species by diffusion and migration occurs radially from the surface, allowing the depletion layer thickness, δ, to be conveniently expressed in terms of the electrode radius r_0 (e.g., $\delta = ar_0$, where a is some numerical constant that depends on the relative contributions of migration and diffusion). For example, it is straightforward to show that for a purely diffusion-controlled response, the concentration of a reactant reaches 90% of its bulk value at a distance of 10 radii from the center of a spherical electrode, i.e., $\delta = 10r_0$[5]. Thus, the lengths r_0 and κ^{-1} are particularly useful for characterizing the relative thicknesses of the depletion layer and the electrical double layer, respectively, surrounding a spherical electrode.

For a macroscopic electrode placed in a solution containing excess supporting electrolyte, κ^{-1} is an insignificant fraction of δ, and the electric field within the double layer has an insignificant effect on the transport of ions to the surface. However, κ^{-1} can become comparable to δ by decreasing either the ionic concentration, C, or the electrode radius, r_0. When $\kappa^{-1} \geq \delta$, the electric field originating at the electrode surface is expected to accelerate or retard the flux of reactant ions to the surface. As a specific example, consider the steady-state electroreduction of an ion A^+ at a positively charged spherical electrode of radius $r_0 = 10$ nm in a solution of total ion concentration equal to 10^{-3} M, Figure 1. For this ionic concentration, $\kappa^{-1} \sim 10$ nm (at 298 K) and the electric field established at equilibrium (zero current) will decay to $\sim 10\%$ of its value at the surface at a distance corresponding to $1.5\kappa^{-1}$ (=15 nm).[6] This value is comparable to the thickness of the depletion layer when a finite current flows across the interface. Assuming a purely diffusion-limited flux, for example, the thickness of the depletion layer can be approximated as $\delta = 10r_0 = 100$ nm (vide supra). Although these estimates of the double layer and depletion layer thicknesses are made under different conditions (i.e., zero and finite current conditions), the reactant ion A^+ will clearly experience a net repulsion as it approaches the positively charged electrode, resulting in a net decrease in the steady-state faradaic current. In this report, numerical and analytical solutions to the transport equations governing the flux of A^+ and associated electrolyte ions are presented that take into account the electric field within the double layer.

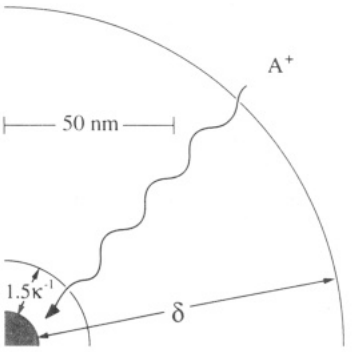

Figure 1. Diagram (drawn to scale) of the relative thicknesses of the diffuse double layer and the depletion layer δ ($\sim 10r_0$) surrounding a 10-nm radius hemispherical electrode immersed in a 10^{-3} M aqueous solution of a 1:1 electrolyte ($\kappa^{-1} \sim 10$ nm). The spherically symmetric diffuse layer thickness is approximated as $1.5\kappa^{-1}$, corresponding to the distance from the surface where the electrostatic potential decays to $\sim 10\%$ of its surface value.

We are particularly interested in electrochemical systems comprised of a redox species and, if charged, its counterion with little or no supporting electrolyte. The most general system we consider is comprised of four chemical species: a redox couple, O^{Z_O}, R^{Z_R} related by

$$O^{Z_O} + (z_O - z_R)e^- \rightarrow R^{Z_R} \quad (1)$$

along with a pair of supporting electrolyte components, X^{Z_X} and Y^{Z_Y}. The systems we examine may contain as few as three species (e.g., O^{Z_O} and X^{Z_X} with the faradaic process producing R^{Z_R} (eq 1)). The problem is solved by presuming that transport and distribution of all species is governed by the Nernst–Planck equation and by classical electrostatics. The resulting set of equations is solved by using a finite-difference methodology. In order to simplify our inquiry we consider only the steady-state in a spherical geometry.

A number of workers[7-11] have considered migration at microelectrodes. With presumption of spherical geometry and the constraint of electroneutrality (corresponding to the limiting case where $r_0\kappa \rightarrow \infty$, i.e., $\kappa^{-1} \ll r_0$), they can obtain some useful analytical expressions for the steady-state flux. Bond et al.[8] also mention (but do not calculate) the infinite dilution limit (the "single-ion case") that occurs when $r_0\kappa \rightarrow 0$ (i.e., $\kappa^{-1} \gg r_0$). In this case, electrostatic ion–ion interaction is negligibly small compared to the interaction with the electric field produced by the charge on the electrode. We shall present the analytic solution for that limiting case since it provides a simple basis for understanding the more complicated systems. We shall also discuss several other limiting cases that have analytic solutions (the aforementioned electroneutrality limit, the trivial diffusion limit attained with an excess of supporting electrolyte, and the zero-current equilibrium (spherical) diffuse double layer). The simulations serve to identify the range of $r_0\kappa$ values appropriate for analytic solutions.

(5) Bard, A. J.; Faulkner, L. R. *Electrochemical Methods*; Wiley: New York, 1980.

(6) The potential distribution around a sphere in an electrolyte is given by $\phi(r)/\phi(r_0) = (r_0/r)\exp(-(r - r_0)\kappa)$ for small values of the surface potential, $\phi(r_0)$.

(7) Kolthoff, I. M.; Ligane, J. J. *Chem. Rev.* **1939**, *24*, No. 1.

(8) Bond, A. M.; Fleischmann, M.; Robinson, J. *J. Electroanal. Chem.* **1984**, *172*, 11.

(9) Amatore, C.; Deakin, M. R.; Wightman, R. M. *J. Electroanal. Chem.* **1987**, *225*, 49.

(10) Morris, R. B.; Fischer, K. F.; White, H. S. *J. Phys. Chem.* **1988**, *92*, 5306.

(11) Oldham, K. B. *J. Electroanal. Chem.* **1988**, *250*, 1.

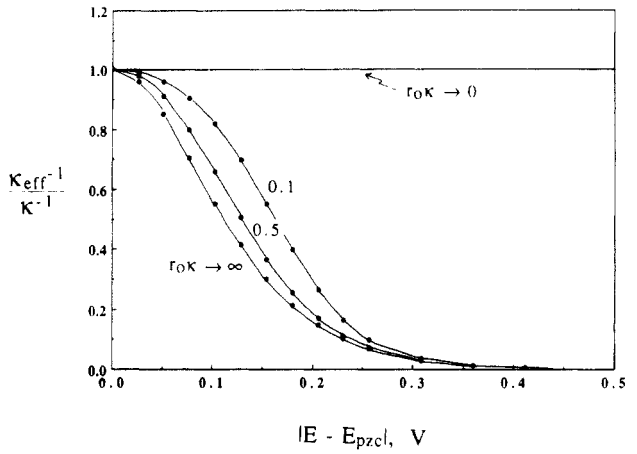

Figure 2. Plot of $\kappa_{eff}^{-1}/\kappa^{-1}$ vs $|E - E_{pzc}|$ for various values of $r_0\kappa$ (from Table 16 of ref 13).

Current–Voltage Behavior in the Limit $r_0\kappa \to 0$

At sufficiently low concentrations of supporting electrolyte or small electrode radii, $r_0\kappa \to 0$ and the number of ions surrounding the electrode is negligible, resulting in an unscreened electrostatic force between the electrode and redox ions. Analysis of this limiting case is developed in three main sections. First, we derive an analytic solution for current–voltage behavior as $r_0\kappa \to 0$. We then report finite-difference simulations of the flux as a function of $r_0\kappa$ and concentration to determine the useful working range of the analytic solution. In the final section, we present examples of steady-state voltammograms expected as $r_0\kappa \to 0$.

A More Precise Definition of the Condition $r_0\kappa \to 0$. The prerequisite condition for an unscreened spherical electrode is that $r_0\kappa \to 0$, where κ^{-1} (the Debye length) is given by[5]

$$\kappa^{-1} = [(kT\epsilon\epsilon_0)/(2c_i z^2 e^2)]^{1/2} \quad (2)$$

In eq 2, c_i is the concentration (molecules/cm^3) of a z:$-z$ electrolyte; ϵ, ϵ_0, e, and kT have their usually significance.

In the Debye–Huckel (D–H) approximation, (i.e., $|E - E_{pzc}| \lesssim 0.02$ V), κ^{-1} corresponds to the distance required for the potential in the diffuse double layer to decrease by a factor of the natural log base; 2.7182818. κ^{-1} is also used in the D–H approximation as a measure of the thickness of the diffuse double layer. The rationale of this construct is based on a hypothetical plate capacitor with each plate bearing a charge equal to the net charge in the diffuse layer. The distance between the capacitor plates can be readily shown[12] to be equal to κ^{-1}.

For $|E - E_{pzc}|$ values larger than ~0.02 V, the diffuse double layer is compressed and the double layer thickness becomes much smaller than κ^{-1}. Thus, the prerequisite condition for an unscreened electrode ought to be $r_0\kappa_{eff} \to 0$, where κ_{eff}^{-1} replaces κ^{-1} as the measure of the diffuse double layer thickness. Using the above-mentioned hypothetical plate capacitor, Loeb, Overbeek, and Wiersema[13] numerically determined values of κ_{eff}^{-1} as a function of $E - E_{pzc}$ and $r_0\kappa$. In Figure 2, we plot values of $\kappa_{eff}^{-1}/\kappa^{-1}$ as a function of $|E - E_{pzc}|$ and for $0 < r_0\kappa < \infty$ (note that $r_0\kappa \to \infty$ corresponds to a planar electrode). As expected, Figure 2 shows that, for all physically reasonable values of $r_0\kappa$, the diffuse layer thickness decreases rapidly as $|E - E_{pzc}|$ increases. In the limit $r_0\kappa \to 0$, the potential profile is entirely a function of electrode radius and there is no electrostatic screening. Figure 2 is useful for estimating the range of $r_0\kappa$ and $|E - E_{pzc}|$ values where the migrational flux of ions is affected by the electrode charge.

In cases where ions are produced by oxidation or reduction of a neutral reactant (see subsequent discussions), the value of κ^{-1} (or κ_{eff}^{-1}) can only be approximated since the definition of κ^{-1} is based on the bulk ion concentration. A crude estimate is to presume that the bulk concentration is approximately equal to the sum of the bulk electrolyte and reactant concentrations. Numerical simulation of the general problem will be used in a later section to establish just how large a value of $r_0\kappa$ can be tolerated without compromising the presumption of no electrostatic screening.

General Current–Voltage Relationship as $r_0\kappa \to 0$. The current–voltage expression is obtained for the situation in which the solution contains both reduced and oxidized forms of a redox couple related by $O^{z_O} + (z_O - z_R)e^- \to R^{z_R}$. For clarity, the superscripts z_O and z_R shall be omitted.

We shall assume that the electron-transfer reaction is governed by Butler–Volmer kinetics:

$$f_e = k_0(C_O^{PET} \exp[-\alpha(F/RT)\eta] - C_R^{PET} \exp[(1 - \alpha) \times (F/RT)\eta]) = k_f C_O^{PET} - k_r C_R^{PET} \quad (3)$$

where f_e is the electron flux ($=i/(z_O - z_R)FA$), k_0 is the standard heterogeneous rate constant, η is the overpotential ($E - E^{0\prime}$), α is the transfer coefficient, and C_O^{PET} and C_R^{PET} are the concentrations of O and R at the plane of electron transfer (PET). Equation 3 assumes that the rate-controlling electron transfer is a one-electron process even if $(z_O - z_R) > 1$. Since the premise of this derivation is that the ion concentration is virtually zero ($r_0\kappa \to 0$), there is no double layer. How then do we define the potential between the electrode and the PET? We shall assume that the location of the PET is equivalent to that of the plane of closest approach of the redox species—roughly equivalent to the distance of the outer Helmholtz plane (OHP) from the electrode in the presence of electrolyte. We shall define μ as the distance between the electrode surface and the PET.

In the absence of ions, the distance dependence of the electric field in a spherical geometry is

$$\mathcal{E}_r = (r_0/r)^2 \mathcal{E}_{r=r_0} \quad (4)$$

The electrostatic potential at the metal surface versus the bulk of solution is

$$\phi_{r=r_0} = -\int_{\infty}^{r_0} \mathcal{E}_r \, dr = r_0 \mathcal{E}_{r=r_0} \quad (5)$$

The difference in potential between the electrode surface and the PET is then

$$\phi_{r=r_0} - \phi_{r=(r_0+\mu)} = -\int_{r_0+\mu}^{\infty} \mathcal{E}_r \, dr = \phi_{r=r_0}(\mu/(r_0 + \mu)) \quad (6)$$

For convenience we shall define

$$\gamma = \mu/(r_0 + \mu) \quad (7)$$

The electrostatic potential, $\phi_{r=r_0}$, may be defined in terms of the applied electrode potential, E:

$$\phi_{r=r_0} = E - E_{pzc} \quad (8)$$

where E_{pzc} is the electrode potential at zero charge (i.e., when $\phi_{r=r_0} = 0$).

Changes in the electrostatic potential between r_0 and $r_0 + \mu$ vary the driving force for electron transfer (eq 3). The operative potential term in the Butler–Volmer equation, η, is the electrode potential and will include the term $(E^{0\prime} - E_{pzc})$ in addition to the electrostatic potential, $\gamma\phi_{r=r_0}$. Thus

$$\eta = \gamma\phi_{r=r_0} - (E^{0\prime} - E_{pzc}) = \gamma(E - E^{0\prime}) - (1 - \gamma)(E^{0\prime} - E_{pzc}) \quad (9)$$

We choose this form since $(E - E^{0\prime})$ is more likely to be well known than $(E - E_{pzc})$. Note that when $\mu \ll r_0$ and $\gamma \to 0$, the value of η is independent of the applied potential, E. (This result, when substituted into eq 3, would appear to indicate that the electron flux becomes a potential independent quantity in the limit $\gamma \to 0$, i.e., $(d\eta/dE)_{\gamma=0} = 0$. However, we will momentarily show that C_O^{PET} and C_R^{PET} are dependent on the electrostatic potential and that the electron flux remains a function of the applied potential through these quantities.) Conversely if $\mu \gg r_0$ and therefore γ

(12) Bockris, J. O'M.; Reddy, A. K. N. *Modern Electrochemistry*; Plenum: New York, 1970.

(13) Loeb, A. L.; Overbeek, J. Th. G.; Wiersema, P. H. *The Electrical Double Layer Around a Spherical Colloid Particle*; MIT Press: Cambridge, MA, 1960.

$\rightarrow$ 1, the change in potential would occur entirely within the region between the electrode surface and the PET and classical behavior would be obtained. Although this condition cannot be attained physically, it is useful to consider it since this behavior is similar to that of a macroscopic electrode in a concentrated electrolyte (i.e., $r_0\kappa \rightarrow \infty$).

The resultant reformulation of the Butler–Volmer expression is

$$f_e = k_0[C_O^{PET} \exp[-\alpha(F/RT)[\gamma(E - E^{0\prime}) - (1 - \gamma) \times (E^{0\prime} - E_{pzc})]] - C_R^{PET} \exp[(1 - \alpha)(F/RT)[\gamma(E - E^{0\prime}) - (1 - \gamma)(E^{0\prime} - E_{pzc})]]] \quad (10)$$

While the underlying concept of this modification is identical with that of the Frumkin correction,[14] there is a significant distinction: we do not presume that the concentration of species at the PET is always in electrostatic equilibrium with the bulk species. However, when $f_e = 0$, C_j^{PET} will be given by the Boltzmann distribution law:

$$C_j^{PET} = C_j^* \exp[-z_j(F/RT)\phi_{r=r_0+\mu}] \quad (11)$$

where C_j^* is the bulk concentration of the jth species. $\phi_{r=r_0+\mu}$ may be obtained from eqs 5 and 6 to give the *equilibrium concentrations* at the PET

$$C_j^{PET} = C_j^* \exp[-z_j(F/RT)(1 - \gamma)\phi_{r=r_0}] = C_j^* \exp[-z_j(F/RT)(1 - \gamma)(E - E_{pzc})] \quad (12)$$

It is trivial to ascertain that eq 10 (with $f_e = 0$) will then reduce to the Nernst equation. Note, at equilibrium the number of electrons assumed in the exponential terms of eq 3 or eq 10 is equal to $(z_O - z_R)$ instead of 1 (as assumed in the rate controlling step).

For the nonequilibrium case (i.e., $f_e \neq 0$), the surface concentrations of C_O^{PET} and C_R^{PET} in the limit of $r_0\kappa \rightarrow 0$ can be obtained by solving for the diffusional-migrational fluxes of O and R. We assume that the transport process is governed by the Nernst–Planck equation:

$$f_j = -D_j(dC_j/dr) + D_j(F/RT)\mathcal{E}_r C_j z_j = -D_j(dC_j/dr) + D_j(F/RT)\mathcal{E}_{r=r_0} r_0(r_0/r^2) C_j z_j \quad (13)$$

Defining a dimensionless interaction energy, W_j, between the electrode and species j,

$$W_j = (F/RT)z_j\mathcal{E}_{r=r_0}r_0 = (F/RT)z_j\phi_{r=r_0} = (F/RT)z_j(E - E_{pzc}) \quad (14)$$

eq 13 becomes

$$f_j = -D_j(dC_j/dr) + D_jC_jW_jr_0/r^2 \quad (15)$$

The equation of continuity at steady-state requires that $4\pi r^2 f_j$ be constant as a function of r. Thus, for a spherical coordinate system:

$$(d/dr)(r^2(-D_j(dC_j/dr) + D_jC_jW_jr_0/r^2)) = 0 \quad (16)$$

The solution to eq 16 for the boundary conditions $C_j = C_j^*$ as $r \rightarrow \infty$ and $C_j = C_j^{PET}$ at $r = r_0 + \mu$ is given by eq 17

$$\frac{C_j}{C_j^*} = 1 + \left[\frac{(C_j^{PET}/C_j^* - 1)(\exp[-W_jr_0/r] - 1)}{\exp[-W_j(1 - \gamma)] - 1}\right] \quad (17)$$

The flux of the jth species to the surface (at $r = r_0 + \mu$) is

$$f_{j,r_0+\mu} = \frac{W_j(1 - \gamma)D_jC_j^*}{(r_0 + \mu)}\left[\frac{\exp[-W_j(1 - \gamma)] - C_j^{PET}/C_j^*}{\exp[-W_j(1 - \gamma)] - 1}\right] \quad (18)$$

Rearranging eq 18 for C_O^{PET} and C_R^{PET} and substituting these into the Butler–Volmer equation (eq 3) yields the general i–E relationship in the limit of $r_0\kappa \rightarrow 0$,

$$f_{e,r_0+\mu} = \{k_fC_O^* \exp[-W_O(1 - \gamma)] - k_rC_R^* \exp[-W_R(1 - \gamma)]\}/\left\{1 + (r_0 + \mu) \times \left[\frac{k_f(1 - \exp[-W_O(1 - \gamma)])}{D_OW_O(1 - \gamma)} + \frac{k_r(1 - \exp[-W_R(1 - \gamma)])}{D_RW_R(1 - \gamma)}\right]\right\} \quad (19)$$

The current–potential behavior predicted by this equation is complex since W_j, k_f, and k_r are potential-dependent (see eqs 3, 9, and 14). We shall discuss some examples of limiting behavior of eq 19 and compute some steady-state voltammograms.

Generalized Limiting Flux. In order to achieve a limiting flux condition, it is usually presumed that either k_f or $k_r \rightarrow \infty$. This limit is straightforward to obtain from eq 19 when $W_j(1 - \gamma) = 0$. Otherwise, for any non-zero value of $W_j(1 - \gamma)$, it is important to examine the potential dependence of the operative rate terms $k_f \exp[-W_O(1 - \gamma)]$ and $k_r \exp[-W_R(1 - \gamma)]$ (eq 20 and 21).

$$k_f \exp[-W_O(1 - \gamma)] = k_f' = k_0 \exp[-(F/RT)z_O(E - E_{pzc}) \times (1 - \gamma)] \exp[-\alpha(F/RT)(\gamma(E - E^{0\prime}) - (1 - \gamma)(E^{0\prime} - E_{pzc}))] \quad (20)$$

$$k_r \exp[-W_R(1 - \gamma)] = k_r' = k_0 \exp[-(F/RT)z_R(E - E_{pzc})(1 - \gamma)] \exp[(1 - \alpha)(F/RT)(\gamma(E - E^{0\prime}) - (1 - \gamma)(E^{0\prime} - E_{pzc}))] \quad (21)$$

The criteria for a change in potential to cause an irreversible oxidation or reduction to proceed are

$$dk_f'/dE < 0 \quad \text{(for reduction)} \quad (22)$$

and

$$dk_r'/dE > 0 \quad \text{(for oxidation)} \quad (23)$$

From eqs 22 and 23 we deduce that in order for an irreversible reduction to occur it is necessary that

$$z_O > -\alpha\mu/r_0 \quad (24)$$

and in order for an irreversible oxidation to occur it is required that

$$z_R < (1 - \alpha)\mu/r_0 \quad (25)$$

Since α, r_0, and μ are always positive, and since the electrode radius is greater than the distance of closest approach of the reactant (i.e., $\mu/r_0 < 1$), it will be virtually impossible to cause reduction of an anion with increasingly negative potential. The explanation is quite simple: the more negative the electrode potential becomes the more difficult it is to bring a negatively charged species to the PET. Analogously we can argue that it will be virtually impossible to cause oxidation of a cation with increasingly positive potentials.

For a reversible process we can presume that k_f and k_r are large enough so that the "1" in the denominator of eq 19 is always negligible. Then, the term of import is the ratio k_r'/k_f' and its dependence upon the applied potential, E. From eqs 20 and 21 we deduce the prerequisite condition in order for a reversible oxidation or reduction to occur in the limit $r_0\kappa \rightarrow 0$:

$$(z_O - z_R) > -\mu/r_0 \quad (26)$$

Since $(z_O - z_R)$ is always positive (= n, the number of electrons involved in the reversible process), and since $\mu/r_0 > 0$, the condition stated by eq 26 will always be met.

If we assume that the condition for achieving a transport-limited current has been met, eq 19 then reduces to:

$$f_{e,r_0+\mu} = \pm(1 - \gamma)C_j^*/((r_0 + \mu)(\exp[W_j(1 - \gamma)] - 1)) \quad (27)$$

A positive sign preceding the right-hand side of eq 27 (with j = "O") corresponds to reduction; a negative sign (with j = "R") corresponds to oxidation. Note that the sign of the flux does not depend upon the sign of W_O or W_R. Note also that the limiting

(14) Frumkin, A. N. *Z. Phys. Chem.* **1933**, *164A*, 121.

current is potential dependent and that dependence may be expressed as a function of W_j that is a linear function of the potential (see eq 14):

$$df_{e,r_0+\mu}/dW_j = \pm f_{e,r_0+\mu}\left(\frac{1}{W_j} - \frac{(1-\gamma)\exp[W_j(1-\gamma)]}{(\exp[W_j(1-\gamma)]-1)}\right) \quad (28)$$

The sign of the coefficient of $f_{e,r_0+\mu}$ can change. Thus $df_{e,r_0+\mu}/dE$ can change sign. Because of the potential dependence of the flux it is possible, as we shall demonstrate, for steady-state voltammograms at microelectrodes to exhibit maxima and/or minima instead of the expected sigmoidal wave form.

When $W_j \rightarrow 0$ (i.e., $E \sim E_{pzc}$, or $z_j = 0$), eq 28 must be expanded, yielding:

$$(df_{e,r_0+\mu}/dW_j)_{W_j\rightarrow 0} = f_{e,r_0+\mu;W_j\rightarrow 0}\frac{(1-\gamma)}{2} \quad (29)$$

Diffusional Limiting Current: $W_j(1-\gamma) = 0$. We have just seen that for an unscreened electrode the mass-transfer-limited flux is not necessarily a potential independent flux. For the case where $W_j(1-\gamma) = 0$, the limiting condition for eq 19 when either C_O^{PET} or $C_R^{PET} \rightarrow 0$ is

$$f_{e,r_0+\mu;W_j(1-\gamma)=0} = \pm D_j C_j^*/(r_0+\mu) \quad (30)$$

The sign will be positive for reduction and negative for oxidation. Equation 30 is the well-known steady-state diffusional limit at large overpotentials to a spherical electrode of radius $r_0 + \mu$.[15]

It is important to consider the experimental conditions that might lead to the limit $W_j(1-\gamma) = 0$ (and thus eq 30) while maintaining the prerequisite condition that $r_0\kappa_{eff} \ll 1$ (see eq 2 and accompanying discussion). Even with a neutral reactant ($z_j = 0$ and therefore $W_j = 0$) and no inert electrolyte, it is, in principle, possible to produce a potential between the electrode and the PET that can generate a net current. As $r_0/\mu \rightarrow 0$ this will be more easily accomplished (see criterion given by eq 26). It is likely, however, that $\mu < 1$ nm, and an electrode with a radius of comparable or smaller dimension will be required to obtain the *purely diffusion-limited flux* given by eq 30.

Despite the unlikelihood that $W_j(1-\gamma) = 0$, it is nevertheless useful and informative to normalize observed currents by a theoretical diffusional limit, $i_{L(diff)}$. The latter serves to normalize electrode area that may be difficult to ascertain for ultrasmall electrodes. Combining eqs 27 and 30 yields the normalized mass-transfer-limited current for large values of η in the limit $r_0\kappa \rightarrow 0$:

$$\frac{f_{e,r_0+\mu}}{f_{e,r_0+\mu;W_j(1-\gamma)=0}} = \frac{i_L}{i_{L(diff)}} = \frac{W_j(1-\gamma)}{\exp[W_j(1-\gamma)]-1} \quad (31)$$

Equation 31 is identical with the electrostatic work term in the Smoluchowski–Debye equation used to calculate homogeneous bimolecular rate constants (see Appendix).

Finite-Difference Simulation. Numerical simulation of the normalized transport-limited flux at large η is reported in this section and compared to analytic values obtained from eq 31. The results obtained allow a useful estimate of the maximum permissible value of $r_0\kappa$ for applying the analytic solution presented above. The simulations also yield the flux for intermediate values of $r_0\kappa$. The model utilizes a finite-difference method to simulate the current and ion distribution occurring at a spherical microelectrode of radius r_0.

The electrochemical reactions considered are the 1 – e⁻ reduction of a singly charged cation ($A^+ + e^- \rightarrow A$) and the 1 – e⁻ oxidation of a singly charged anion ($A^- \rightarrow A + e^-$). The solution contains reactant (A^+ or A^-) and a 1:1 electrolyte that shares a common counterion with the reactant. The spherical working electrode is assumed to be surrounded by a large concentric spherical counterelectrode, maintaining a radial flux under all conditions. Nernst–Planck transport (eq 13) is presumed.

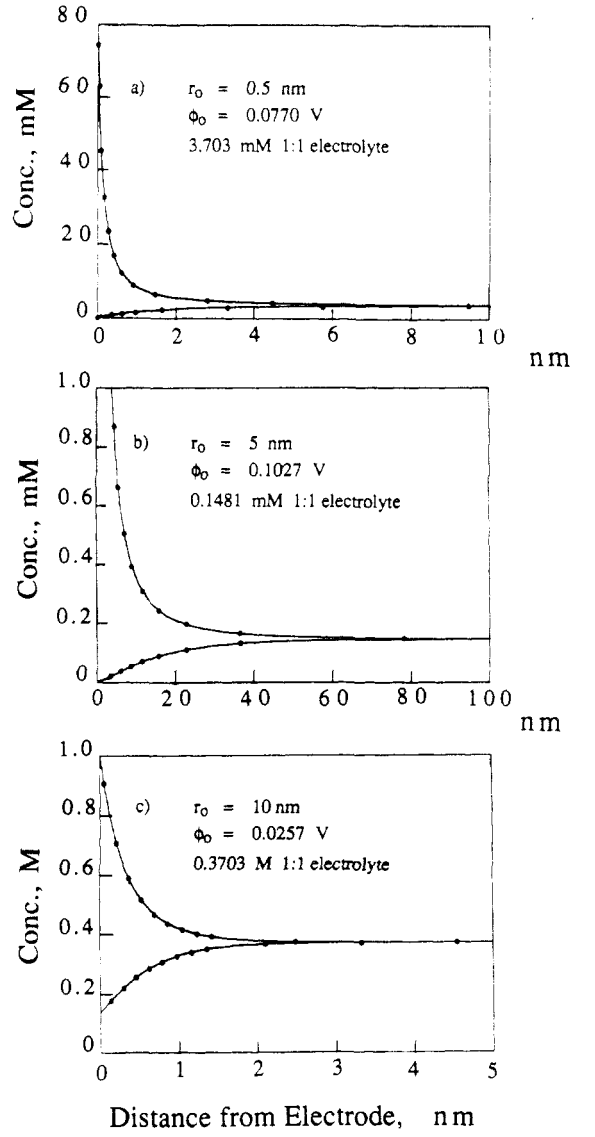

Figure 3. Simulated diffuse double layer concentration profiles surrounding a spherical electrode in a 1:1 aqueous electrolyte. The surface potential (vs E_{pzc}), electrolyte concentration, and electrode radius for each simulation are indicated in the figures. The points correspond to numerical values tabulated in ref 13.

The finite-difference program calculates the time-dependent fluxes and concentrations of all species by following a potential step to the electrode at $t = 0$. Initially, the electrode is assumed to be uncharged with respect to the solution, and all species are distributed uniformly throughout the solution. At $t = 0$, a potential of +0.1 V versus E_{pzc} is applied to the electrode. The potential step is assumed to be sufficiently large to cause the mass-transfer-limited reduction (or oxidation) of A^+ (or A^-) at the limiting current plateau, i.e., C_{A^+} or $C_{A^-} = 0$ as $r \rightarrow r_0$.

The change in the electric field at any point in the solution gives rise to a time-dependent electric field, which is represented by

$$\frac{d\mathcal{E}}{dt} = -\frac{F\sum f_j z_j}{\epsilon\epsilon_0} - \frac{F f_{e,r_0+\mu}}{\epsilon\epsilon_0}\left(\frac{r_0}{r}\right)^2 \quad (32)$$

where $f_{e,r_0+\mu}$ is the flux of electrons into the electrode. Only the final steady-state fluxes are reported here.

The digital simulation utilizes an exponentially expanding grid[16,17] and a variation of the DuFort Frankel algorithm[18] in order

(15) Equation 30 and all preceding equations, in fact, are derived for an electrode of radius r_0. The distance μ that appears in the term $(r_0 + \mu)$ in eq 30 results from applying the boundary condition, $C(r) = C_j^{PET}$ at $r = r_0 + \mu$, in solving for the flux (corresponding to the closest approach of the reactant to the surface).

(16) Joslin, T.; Pletcher, D. *J. Electroanal. Chem.* **1974**, *49*, 171.
(17) Feldberg, S. W. *J. Electroanal. Chem.* **1981**, *127*, 1.

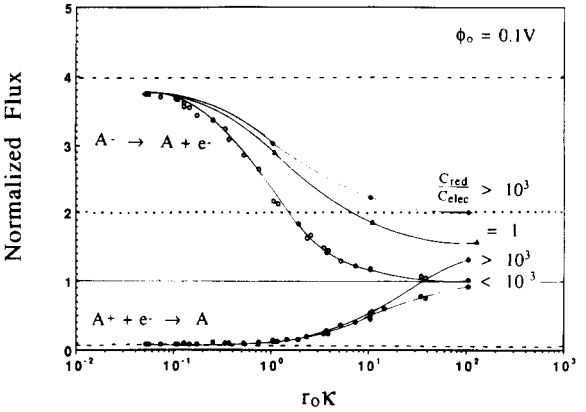

Figure 4. Normalized steady-state flux as a function $r_0\kappa$ for various values of C_{redox}/C_{elec}. The diffusion-limited current in the absence of migration, $i_{L(diff)}$, is equal to $4\pi nFDC^*r_0$. The dashed lines ($i_L/i_{L(diff)}$ = 3.97 and 0.081) correspond to eq 31, the analytic value of the flux in the limit $r_0\kappa \to 0$. The dotted line ($i_L/i_{L(diff)} = 2$) corresponds to the diffusion–migration limit (eq 38) when the supporting electrolyte concentration is much smaller than the redox species concentration, $C_{redox}/C_{elec} \gg 1$.

to enhance simulation speed. A detailed description of the simulations will be presented in a forthcoming publication. The accuracy of the model and the numerical calculations was verified by comparison with known solution.

Figure 3a–c shows a comparison of the equilibrium (zero current) ion concentration profiles generated by our numerical simulation (solid lines) with the numerically calculated results of Loeb et al.[13] (points) for 0.5, 5.0, and 10.0 nm radius spherical electrodes. The bulk concentration of the 1:1 electrolyte (0.148–372 mM) and the surface potential (0.026–0.103 V) used in the simulations are indicated in each figure. In all cases, excellent agreement (within 1%) is obtained between our simulations and the numerical results of Loeb et al. (obtained by numerical solution of the Poisson–Boltzmann equation for a charged sphere).

Simulated Fluxes. Transport-limited steady-state currents obtained from finite-difference simulations corresponding to the $1 - e^-$ reduction of a cation ($A^+ + e^- \to A$) and the $1 - e^-$ oxidation of an anion ($A^- \to A + e^-$) are shown in Figure 4. In each system, we assume a 1:1 supporting electrolyte, an applied potential of +0.1 V versus E_{pzc}, and zero product concentration in the bulk. The results are plotted in Figure 4 as a function of $r_0\kappa$, where κ is based on the sum of the bulk concentrations of reactant, counterion, and supporting electrolyte. Each line in Figure 4 corresponds to a different ratio of the concentrations of reactant (A^+ or A^-) to supporting electrolyte, C_{redox}/C_{elec}.

Numerical values of limiting currents have been normalized to the current expected for a purely diffusion-controlled reaction at a sphere of radius r_0, i.e., $i_{L(diff)} = 4\pi nFDC^*r_0$ where C^* is the bulk reactant concentration). Thus, the horizontal line at $i/i_{L(diff)} = 1$ in Figure 4 corresponds to the oxidation or reduction of a neutral reactant at large overpotential.

Figure 4 shows that a deviation from classical diffusion-limited current is observed as $r_0\kappa$ decreases and/or as C_{redox}/C_{elec} increases. This complex behavior arises partly because the diffusion layer and the double layer have comparable dimensions.

(i) Migration Resulting from Depletion of Reactant Ions at the Electrode. At large $r_0\kappa$ (e.g., corresponding to a macroscopic electrode), the current for either the reduction of A^+ or the oxidation of A^- to the neutral A increases to a value approximately twice as large as the purely diffusional current when the electrolyte concentration becomes appreciably smaller than the reactant concentration, i.e., when $C_{redox}/C_{elec} > 10^2$ (Figure 4). This behavior was first described quantitatively by Heyrovsky[19] and Ilkovic[20] and more recently addressed in context of microelectrode behavior in solutions of low ionic strength.[7-11] In the limit of little or no supporting electrolyte, the system can be approximated as containing three species in solution, the charged reactant, $j = 1$, its corresponding counterion, $j = 2$, and the neutral redox product, $j = 3$. Solution electroneutrality requires that

$$C_1z_1 + C_2z_2 = 0 \tag{33}$$

and

$$\frac{dC_1}{dr}z_1 + \frac{dC_2}{dr}z_2 = 0 \tag{34}$$

Using eq 13 to define the fluxes of reactant and counterion:

$$f_1 = -D_1\frac{dC_1}{dr} + D_1\frac{F}{RT}\mathcal{E}C_1z_1 \tag{35}$$

$$f_2 = 0 = -D_2\frac{dC_2}{dr} + D_2\frac{F}{RT}\mathcal{E}C_2z_2 \tag{36}$$

and substituting eqs 33, 34, and 36 into eq 35 yields the steady-state reactant flux:

$$f_1 = -D_1\frac{dC_1}{dr}\left(1 - \frac{z_1}{z_2}\right) \tag{37}$$

Combining eq 37 with the continuity equation for a spherical system ($(d/dr)(r^2f_j) = 0$) and integrating using the boundary conditions $C \to C^*$ as $r \to \infty$ and $C = 0$ at $r = r_0$ yields the expected transport-limited current:

$$i_L = 4\pi nFDC^*r_0\left(1 - \frac{z_1}{z_2}\right) \tag{38}$$

In solutions containing a monovalent reactant (A^+ or A^-) and a monovalent counterion of opposite charge (X^- or X^+), the limiting current (eq 38) for either cation reduction or anion oxidation should increase by a factor of 2 relative to the diffusion-limited current in the presence of excess supporting electrolyte, $i_{L(diff)}$.

The dotted line in Figure 4 shows the asymptotic limiting value of 2 that the normalized current approaches as C_{redox}/C_{elec} increases. We find that $i_L/i_{L(diff)}$ for the oxidation of A^- equals 2 for $C_{redox}/C_{elec} \gg 10^3$ and $r_0\kappa > 10$. However, for the same values of C_{redox}/C_{elec} and $r_0\kappa$, $i_L/i_{L(diff)}$ for the reduction of A^+ is significantly smaller, ~1.32, than the expected value of 2. We show in the following section that this deviation is due to electrostatic repulsion between the positively charged electrode (ϕ_0 = 0.1 V) and A^+.

(ii) Migration Resulting from the Electrostatic Field Originating at the Electrode Surface. For $r_0\kappa < 50$, the limiting current deviates from the diffusional currents even when the supporting electrolyte concentration is considerable larger than the redox active concentration. For example, the current corresponding to the oxidation of A^- at $r_0\kappa = 10$ and $C_{redox}/C_{elec} = 10^{-3}$ is ~20% *larger* than the purely diffusion-controlled value. Conversely, at a similar concentration ratio the reduction of A^+ yields a current that is 55% *smaller* than the purely diffusion-controlled value. We ascribe these deviations from a purely diffusional response to electrostatic double layer forces acting on the reactant within the depletion layer. Qualitatively, the flux of an anionic reactant to a positively charged electrode is expected to be increased, resulting from electrostatic attraction. Conversely, the flux of cationic reactant would be decreased. This behavior is observed in Figure 4 for the reaction of +1 and −1 species at a positively charged electrode (ϕ_0 = 0.1 V).

As anticipated, the effect of the electrical double layer on migrational currents becomes more pronounced as $r_0\kappa$ decreases. This behavior reflects the relative dimensions of the double layer with respect to the depletion length, which in turn is determined by the electrode radius and electrolyte concentration (see Figure 1). When $\kappa^{-1} \ll r_0$ (i.e., $r_0\kappa \to \infty$), the thickness of the double layer is insignificant compared to the thickness of the diffusion layer, and reactant ions do not experience an electrostatic force until they are in the immediate vicinity of the electrode. Under these circumstances, reactant ions are driven by the concentration

(18) DuFort, E. C.; Frankel, S. P. *Math. Tables Aids Comp.* **1953**, *7*, 135.
(19) Heyrovsky, J. *Archiv. Hem. Farm.* **1934**, *8*, 11.
(20) Ilkovic, D. *Collec. Czech. Chem. Commun.* **1934**, *6*, 498.

TABLE I: Normalized Mass-Transfer Currents as $r_0\kappa \rightarrow 0$[a]

reaction	analytic[b]	finite difference simulation[c]
$A^- \rightarrow A + e^-$	3.97	3.95
$A^+ + e^- \rightarrow A$	0.081	0.081

[a] The electrode potential is +0.1 vs E_{pzc}. [b] Equation 31. [c] Simulation conditions: r_0 <0.5 nm; C^* = 1 mM; no supporting electrolyte.

gradient from the bulk solution to the surface across an electroneutral depletion layer. Conversely, when $\kappa^{-1} \geq r_0$ (i.e., $r_0\kappa \rightarrow 0$), the thickness of the diffusion layer is much smaller than the thickness of the double layer, where the electric field can cause an increase or decrease in the transport limited current.

As $r_0\kappa \rightarrow 0$, the normalized mass-transport-limited current asymptotically approaches limiting values for the reduction of A^+ and for the oxidation of A^-. The asymptotic limits are given in Table I and compared to the exact analytic solution (eq 31) obtained by using $\phi_0 = 0.1$ V and $z_j = -1$ and +1. The disparity between these two values is less than 1%, demonstrating the accuracy of the simulations.

Voltammetry at Microelectrodes as $r_0\kappa \rightarrow 0$. We now describe the overall steady-state voltammetric behavior of spherical microelectrodes in the limit $r_0\kappa \rightarrow 0$. Before discussing the results, it is useful to consider the applicability of the analytic theory in predicting the behavior of real electrochemical systems. From Figure 4, we find that normalized flux predicted by eq 31 for the oxidation of A^- (which is exact in the limit $r_0\kappa \rightarrow 0$) is closely approximated by the simulated fluxes when $r_0\kappa < 0.1$. For the reduction of A^+, the analytic and simulated values coincide when $r_0\kappa < 1.0$. Thus, the analytic solution for the overall current–voltage relationship (eq 19) can be applied to approximate the behavior of these particular systems when $r_0\kappa$ is less than the aforementioned values. As a specific example, a 30-nm radius electrode in an aqueous solution (298 K) containing ~0.1 mM A^+X^- corresponds to $r_0\kappa = 1$. The voltammetric behavior of this system would, thus, be described by eq 19.

In general, the useful working range of eq 19 is dictated by both the sign and magnitude of the dimensionless interaction term, W_j (for both O and R), as well as $r_0\kappa$. Equation 14 shows that W_j is proportional to both z_j and E. Thus, double layer effects on transport-limited fluxes become more pronounced as W_j increases. However, it will become more difficult to maintain the requisite condition that $r_0\kappa_{eff} \rightarrow 0$ as either of these two parameters is increased since higher potentials or a higher ion charge results in increased screening of the electrostatic field (for example, see Figure 2 and Figure 3). In effect, an increase in W_j is offset by an increase in the screening of the field.

For $r_0\kappa > 1$, the electrode charge is partially screened and eq 19 is no longer strictly applicable. However, from Figure 4 we note that the flux expected for a totally screened electrode is not always obtained for values of $r_0\kappa$ as large as 100. Thus, it is plausible, and even likely in certain instances, that the electrical double layer has a measurable effect on the voltammetric behavior of electrodes of μm dimension.

Equation 19 was used to calculate the voltammetric behavior expected for the following redox systems:

$$A^+ + e^- \rightleftharpoons A \quad \text{(Figure 5)} \tag{39}$$

$$A^+ \rightleftharpoons A^{2+} + e^- \quad \text{(Figure 6)} \tag{40}$$

$$A \rightleftharpoons A^{2+} + 2e^- \quad \text{(Figure 7)} \tag{41}$$

Each system exemplifies different types of behavior resulting from migration within the double layer. We calculate the voltammograms assuming that both halves of the redox couple are soluble in solution, and that the product (right-hand side of eqs 39, 40, or 41) has a zero bulk concentration. In plotting the voltammetric curves, we set $E^{0\prime}$ equal to 0.0V vs an unspecified reference electrode, allowing numerical values of E_{pzc} to be defined vs $E^{0\prime}$. Each voltammogram is normalized to the diffusion-limited flux given by eq 30. We assume that $D_O = D_R$ (= D) and that the transfer coefficient, α, is equal to 0.5.

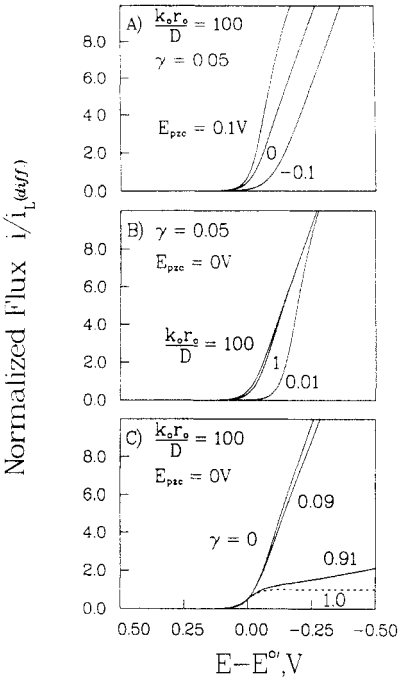

Figure 5. Theoretical voltammograms calculated from eq 19 for the reaction $A^+ + e^- \rightarrow A$ as a function of (A) E_{pzc}, (B) k_0r_0/D, and (C) γ. The formal redox potential of the couple A^+/A, $E^{0\prime}$, is set equal to 0 V vs an arbitrary reference electrode. The dotted line in C indicates the diffusion-limited reversible voltammogram when $\gamma \rightarrow 0$.

In addition to D and α, there are five independent parameters in eqs 19–21 that affect the shape of the voltammetric response: $(E_{pzc} - E^{0\prime})$, W_O, W_R, k_0r_0/D, and γ. The first three of these ($(E_{pzc} - E^{0\prime})$, W_O, and W_R) are determined completely by thermodynamic quantities of the system and by the reactant and product ion charges. The remaining two parameters (k_0r_0/D and γ) are associated with electron-transfer kinetics and are dependent on the electrode size.

The term k_0r_0/D is the ratio of the heterogeneous electron-transfer rate to the mass-transfer rate (D/r_0) at a spherical electrode in the absence of migration and convection. We will examine voltammetric responses for k_0r_0/D = 100, 1, and 0.01, which correspond to reversible, quasi-reversible, and irreversible electron-transfer reactions at macroscopic spherical electrodes in the presence of excess supporting electrolyte. Values of the dimensionless electron-transfer distance, γ, are constrained by realistic values of r_0 and μ and by the presumed condition $r_0\kappa \rightarrow 0$. We have observed from numerical simulations that the condition for an unscreened electrode is satisfied when $r_0\kappa < 0.1$. Since electrolyte concentrations are typically between 1 and 10^{-4} M, this limitation requires r_0 values between 0.3 and 30 nm. However, it is unlikely that electrodes with dimensions less than 1 nm can be fabricated. From our definition of γ (eq 7), and assuming an electron-transfer distance μ between 0.2 and 1 nm, we find ~0.25 < γ <0.007.

Figure 5 shows the voltammetric response expected for the 1 – e^- reduction of A^+ (eq 39) as a function of $(E_{pzc} - E^{0\prime})$, k_0r_0/D, and γ. For comparison, we include the sigmoidal-shaped voltammogram (dashed curve in Figure 5C) that corresponds to the classical diffusion-limited reduction (i.e., when $W_j(1 - \gamma) \rightarrow 0$ for both O and R). The predominant factor in determining the shape of the voltammetric curves in Figure 5 is migration of A^+ in response to the electrode charge, which depends on the relative values of E and E_{pzc}. In Figure 5A, we plot voltammograms as a function of $(E_{pzc} - E^{0\prime})$ for $k_0r_0/D = 10^2$ and γ = 0.05. For $(E_{pzc} - E^{0\prime}) = 0$, the reduction of A^+ is greatly enhanced (relative to the purely diffusion-limited current) when the E is more negative than E_{pzc}, reflecting an attractive force between the negative electrode and positive ion. Conversely, when E is moved more positive than E_{pzc}, electrostatic repulsion between the reactant

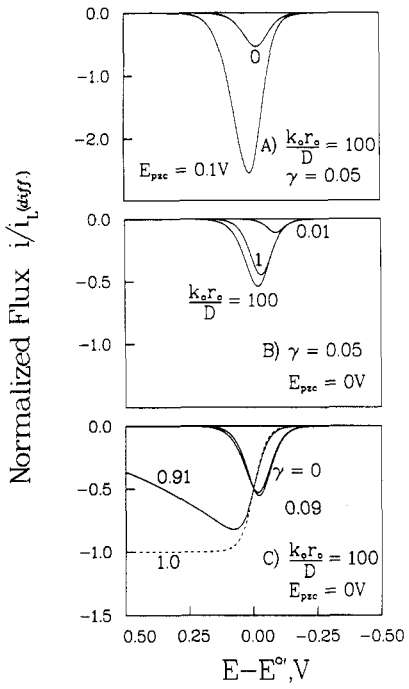

Figure 6. Theoretical voltammograms calculated from eq 19 for the reaction $A^+ \rightarrow A^{2+} + e^-$ as a function of (A) E_{pzc}, (B) k_0r_0/D, and (C) γ. The formal redox potential of the couple A^+/A, $E^{0\prime}$, is set equal to 0 V vs an arbitrary reference electrode. The dotted line in C indicates the diffusion-limited reversible voltammogram when $\gamma \rightarrow 0$.

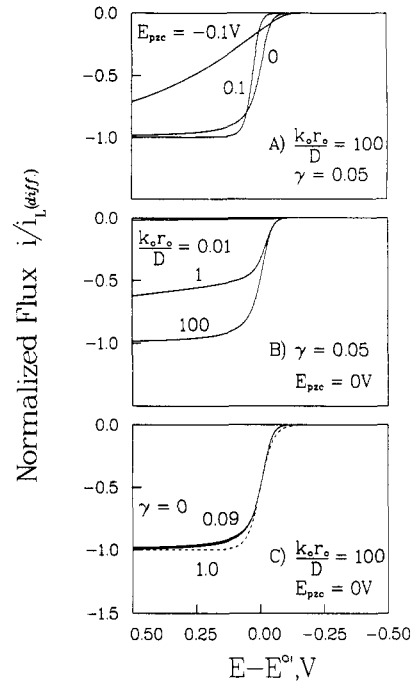

Figure 7. Theoretical voltammograms calculated from eq 19 for the reaction $A \rightarrow A^{2+} + 2e^-$ as a function of (A) E_{pzc}, (B) k_0r_0/D, and (C) γ. The formal redox potential of the couple A^+/A, $E^{0\prime}$, is set equal to 0 V vs an arbitrary reference electrode. The dotted line in C indicates the diffusion-limited reversible voltammogram when $\gamma \rightarrow 0$.

and electrode decreases the magnitude of the current. Voltammograms for $(E_{pzc} - E^{0\prime}) = 0.1$ and -0.1 V, also shown in Figure 5A, can be qualitatively explained in a similar fashion.

In Figure 5B, we show that the dimensionless heterogeneous rate, k_0r_0/D, affects the shape of the voltammetric behavior only at potentials corresponding to the foot of the wave. We note from the criterion for a irreversible reduction, $z_O > -\alpha\mu/r_0$ (eq 24), that it will always be possible to affect the reduction of A^+, regardless of how small k_0r_0/D becomes.

At sufficiently large negative overpotentials, migration of A^+ toward the surface becomes rate limiting. The transport limited flux is given by eq 31, which for large overpotentials reduces to

$$i_L/i_{L(diff)} = -W_j(1 - \gamma) \tag{42}$$

Equation 42 indicates the mass-transfer-limited current increases linearly with increasing W_j and therefore with increasing overpotential (eq 14, Figure 5).

Figure 6 shows voltammograms for the $1 - e^-$ oxidation of A^+ to A^{2+} (eq 40) for the same potential range and values of E_{pzc} as in Figure 5. Here, the voltammograms have a skewed bell shape resulting from electrostatic repulsion of A^+ from the electrode at positive potentials that normally correspond to the diffusion-limited current plateau. The criterion required for irreversible oxidation, $z_R < (1 - \alpha)\mu/r_0$ (eq 25), is not satisfied, resulting in the mass-transfer-limited current (eq 31) being suppressed to negligible values at potentials sufficiently positive of E_{pzc}. For instance, at an electrode where $E_{pzc} - E^{0\prime} = 0$, the limiting current at $E = 0.2$ V is reduced to 0.3% of the purely diffusion-limited current. When $E_{pzc} - E^{0\prime} < 0$, electrostatic repulsion effectively eliminates the voltammetric wave (Figure 6A). Decreasing the value of k_0r_0/D has a similar effect on the wave shape as shifting E_{pzc} to potentials more negative than $E^{0\prime}$. However, a shift of -0.2 V in E_{pzc} causes a larger decrease in the voltammetric currents than a 10^4 decrease in k_0r_0/D (compare Figures 6A and 6B).

The wave shapes observed in Figures 5 and 6 and their dependencies on E_{pzc} result from the strong dependence of the migrational flux of both reactant and product on the electrostatic potential. To a first approximation, the forward and reverse electron-transfer rates k_f $(= k_0 \exp[-\alpha(F/RT)\eta])$ and k_r $(= k_0 \exp[(1 - \alpha)(F/RT)\eta])$ are essentially potential-independent values. This occurs because η has a weak dependency on E for realistically small values of γ (see eq 9 and accompanying discussion). To illustrate this, we show in Figure 5C and Figure 6C that varying γ between 0 and 0.1 has a negligible effect on the wave shape. Thus, the voltammetric response is weakly dependent on μ (the distance of closest approach). In the limit $\mu \rightarrow 0$, and thus $\gamma \rightarrow 0$, k_f and k_r are truly potential-independent rate constants. It is important to note, however, that even with this limiting condition, a potential change can produce currents because of changes induced in C_O^{PET} and C_R^{PET}.

Figure 7 shows voltammograms corresponding to the $2e^-$ oxidation of A (eq 41). In this case, $W_R = 0$ and $C_O^* = 0$ (the bulk concentration of A^{2+} is zero), and eq 19 reduces to:

$$f_{e,r_0+\mu} = \frac{-k_r C_R^*}{1 + \frac{(r_0 + \mu)}{D}\left[\frac{k_f(1 - \exp[-W_O(1 - \gamma)])}{W_O(1 - \gamma)} + k_r\right]} \tag{43}$$

For the same reason discussed for the above examples, k_r and k_f are weakly dependent on E. Thus, when W_O is very negative (in this case, when $(E - E_{pzc})$ is very negative), at large negative potentials, $(1 - \exp[-W_O(1 - \gamma)])/(W_O(1 - \gamma)) \rightarrow \infty$ and $f_e \rightarrow 0$. This limit is obtained regardless of electron-transfer reversibility. In effect, the back-reaction is increased because of strong electrostatic attraction of the reaction product, A^{2+}, to the negatively charged surface.

At large positive potentials, $(k_f(1 - \exp[-W_O(1 - \gamma)]))/(W_O(1 - \gamma)) \ll k_r$ and the flux is given by

$$f_{e,r_0+\mu} = \frac{-k_r C_R^*}{1 + (r_0 + \mu)\frac{k_r}{D}} \tag{44}$$

For a reversible electron-transfer reaction (i.e., $k_0r_0/D \gg 1$), eq 44 reduces to eq 30, and the diffusion-controlled limiting current is obtained. This situation is shown in Figure 7A for several values of E_{pzc} and for $k_0r_0/D = 100$.

For an irreversible reaction (i.e., $k_0r_0/D \ll 1$), eq 44 reduces to

$$f_{e,r_0+\mu} = -k_r C_R^* \tag{45}$$

Recalling that k_r is essentially constant, eq 45 states that the

current at large overpotentials is independent of applied potential and proportional to the standard heterogeneous rate constant, k_0. Combining the limiting cases for large positive ($f_e = -k_r C_R^*$) and negative ($f_e \to 0$) overpotentials indicates that the i–E curve should have the sigmoidal shape shown in Figure 7B. It is particularly interesting to note that the limiting current plateau observed for small values of $k_0 r_0/D$ does not result from a mass-transfer limitation.

Conclusions

The numerical simulation and analytic expressions presented above demonstrate that a deviation from classical diffusion–migration-limited currents is expected as $r_0\kappa$ decreases. This deviation results from an increased dependence of mass-transfer and electron-transfer kinetics on the electric field within the electrical double layer. The numerical results (Figure 4) suggest that these effects become significant for $r_0\kappa < 100$.

The voltammetric response of a spherical electrode as $r_0\kappa \to 0$ is nonclassical in that a mass-transfer-limiting current plateau is not expected for the reduction or oxidation of a charged or neutral reactant. The shape of the voltammogram depends on E_{pzc} (vs $E^{0\prime}$), the charge of both reactant and product, as well as the distance of closest approach to the electrode surface, μ. Because of the dependence of the voltammetric currents on E_{pzc} and μ, experimental voltammograms may have a measurable dependence on the metal workfunction (and other parameters affecting E_{pzc}) and the radii of redox species.

It is unlikely that the limiting behavior expected as $r_0\kappa \to 0$ can be experimentally examined at an individual spherical (or disk) electrode. To obtain the asymptotic limit below $r_0\kappa \sim 1$ would require a 30-nm sphere in a solution containing less than 10^{-4} M ionic concentration. The difficulty in fabricating such a small spherical electrode, as well as that of measuring an exceedingly small current ($< 10^{-11}$ A), would likely preclude a systematic study. Despite the technical difficulties associated with investigating *individual* spherical electrodes in the limit $r_0\kappa \to 0$, the results presented here are applicable to several types of submicron redox substrates that have spherical or quasi-spherical geometries. In particular, the rate of redox reactions at metal colloids,[21,22] supported catalysts,[23] and small semiconductor particles[24] of nanometer radii may show a significant dependence on the particle size.

It is also possible to fabricate a microband electrode with a critical dimension (width) of the order of several nanometers. Microband electrodes are well-suited for investigating voltammetry as a function of $r_0\kappa$ since one microscopic dimension (width) can be varied over several orders of magnitude, while the second dimension (length) can be maintained at a macroscopic dimension, avoiding problems associated with the measurement of vanishingly small currents. We have previously reported on voltammetry of Pt band electrodes of width 2 to 50 nm in solutions containing 0.1 M 1:1 supporting electrolyte and ~10 mM neutral or charged reactant. These conditions correspond to $0.5 < r_0\kappa < 12$.[25,26] It is therefore worthwhile to qualitatively compare the anticipated voltammetric behavior of a microband electrode with a spherical electrode in the limit of $r_0\kappa \to 0$. Approximating a microband by a hemicylinder, the potential and concentration profiles can be shown to vary as ln (r), as opposed to r^{-1} for spherical geometry. It is thus expected that both the double layer and depletion layer will increase at a hemicylinder to approximately the same extent, relative to their values for a sphere of similar radius. From preliminary numerical simulations, we have found that the dependence of normalized mass-transfer-limited flux on $r_0\kappa$ at a hemicylinder electrode closely parallels the results shown in Figure 4 for a spherical electrode. A detailed study of the effect of double layer fields on the voltammetric behavior of hemicylinder electrodes is currently in progress.

Acknowledgment. We gratefully acknowledge mathematical assistance provided by Dr. Michael C. Armijo, Biology Dept., Brookhaven National Laboratory. Financial support for this work was provided by the Office of Naval Research Young Investigator Program and the Division of Chemical Sciences, United States Department of Energy, Washington, DC (contract No. DE-AC02-76CH00016).

Appendix

Derivation of the Normalized Flux to a Spherical Microelectrode (Eq 31) from Diffusion-Controlled Bimolecular Reaction Rate Theory. An alternative and more intuitive approach in analyzing the transport-limited flux (large η) at microelectrodes in the limit $r_0\kappa \to 0$ is to treat the electrode as a small stationary sphere (i.e., an ion) that reacts with freely diffusing reactant in a bimolecular collision. The rate constant of such a reaction between ions in an infinitely dilute solution was originally considered by Debye[27] using Smoluchowski's method[28] and shown to be dependent on the charges of the two reactants.

$$k_D = 4\pi N_A (D_A + D_B)(r_A + r_B)\frac{W}{\exp(W) - 1} \qquad \text{(A1)}$$

$$W = \frac{z_A z_B e^2}{4\pi\epsilon\epsilon_0 kT(r_A + r_B)}$$

A and B represent the reacting ions with diffusivities D_A and D_B and radii r_A and r_B, respectively. The factor $W/(\exp(W) - 1)$ in eq A1 corresponds to the work required in bringing charged reactants together.

The steady-state flux of an ionic redox species to a charged spherical electrode at large overpotentials can be obtained from eq A1 by letting B represent a stationary electrode ($D_B = 0$ and $r_B = r_0$) to which redox species A is diffusing. The radius of A is equivalent to the thickness μ (the distance of the plane of electron transfer, PET, from the electrode surface). The effective "valency" of the electrode, z_{elec}, is given by

$$z_{elec} = 4\pi\epsilon\epsilon_0(E - E_{pzc})r_0/e^- \qquad \text{(A2)}$$

Combining eqs A1 and A2 yields the expected current at a spherical electrode:

$$i_L = 4\pi nFC^* D_A(r_0 + \mu)\frac{W(1 - \gamma)}{\exp[W(1 - \gamma)] - 1} \qquad \text{(A3)}$$

If either the electrode or reactant is uncharged, then:

$$i_{L(diff)} = 4\pi nFC^* D_A(r_0 + \mu) \qquad \text{(A4)}$$

which is the diffusional current to a spherical electrode. Combining eqs A3 and A4 yields the normalized current as $r_0\kappa \to 0$:

$$\frac{i_L}{i_{L(diff)}} = \frac{W(1 - \gamma)}{\exp[W(1 - \gamma)] - 1} \qquad \text{(A5)}$$

which is identical with eq 31 in the text.

The enhancement or inhibition of bimolecular rates predicted by Debye results from the electrostatic force between the reactant ions. In general, because ions in solution have a relatively low charge (+4 to −4), bimolecular-transport-controlled rate constants in aqueous solutions do not vary by more than a factor of 3 or 4 from the diffusion-controlled rate constant for uncharged species. In contrast, the charge of a spherical electrode, z_{elec}, can be potentiostatically controlled and set to exceeding large values. For example, at 0.1 V vs E_{pzc}, z_{elec} for a 10-nm electrode is +54 and the normalized flux obtained from eq A5 for the oxidation of a monovalent cation is 0.081.

(21) Fleischmann, M.; Ghoroghchian, J.; Rolison, D.; Pons, S. *J. Phys. Chem.* **1986**, *90*, 6392.
(22) Leland, J. K.; Bard, A. J. *J. Phys. Chem.* **1987**, *91*, 5076.
(23) Sobczynski, A.; Bard, A. J.; Campion, A.; Fox, M. A.; Mallouk, T.; Webber, S. E.; White, J. M. *J. Phys. Chem.* **1987**, *91*, 3316.
(24) Liu, C. Y.; Bard, A. J. *J. Phys. Chem.* **1989**, *93*, 3232.
(25) The current to a microband electrode of width w is given by the flux to a hemicylinder of radius $w/4$ (ref 26).
(26) Szabo, A.; Cope, D. K.; Tallman, D. E.; Kovach, P. M.; Wightman, R. M. *J. Electroanal. Chem.* **1987**, *217*, 285.
(27) Debye, P. *Trans. Electrochem. Soc.* **1942**, *82*, 265.
(28) Smoluchowski, M. V. *Z. Phys. Chem.* **1917**, *92*, 129.